SUPPLEMENTARY FIGURE LEGENDS

A

Cohort	Age at first dose	No. of NMU doses	Rats with tumors	Tumors per rat	Days from NMU to tumor
1	53	1	0/10		
2	49	1	4/4	1	~75
3	35	3	10/10	1-8	~55
4	35	1	9/10	1-4	~40-80

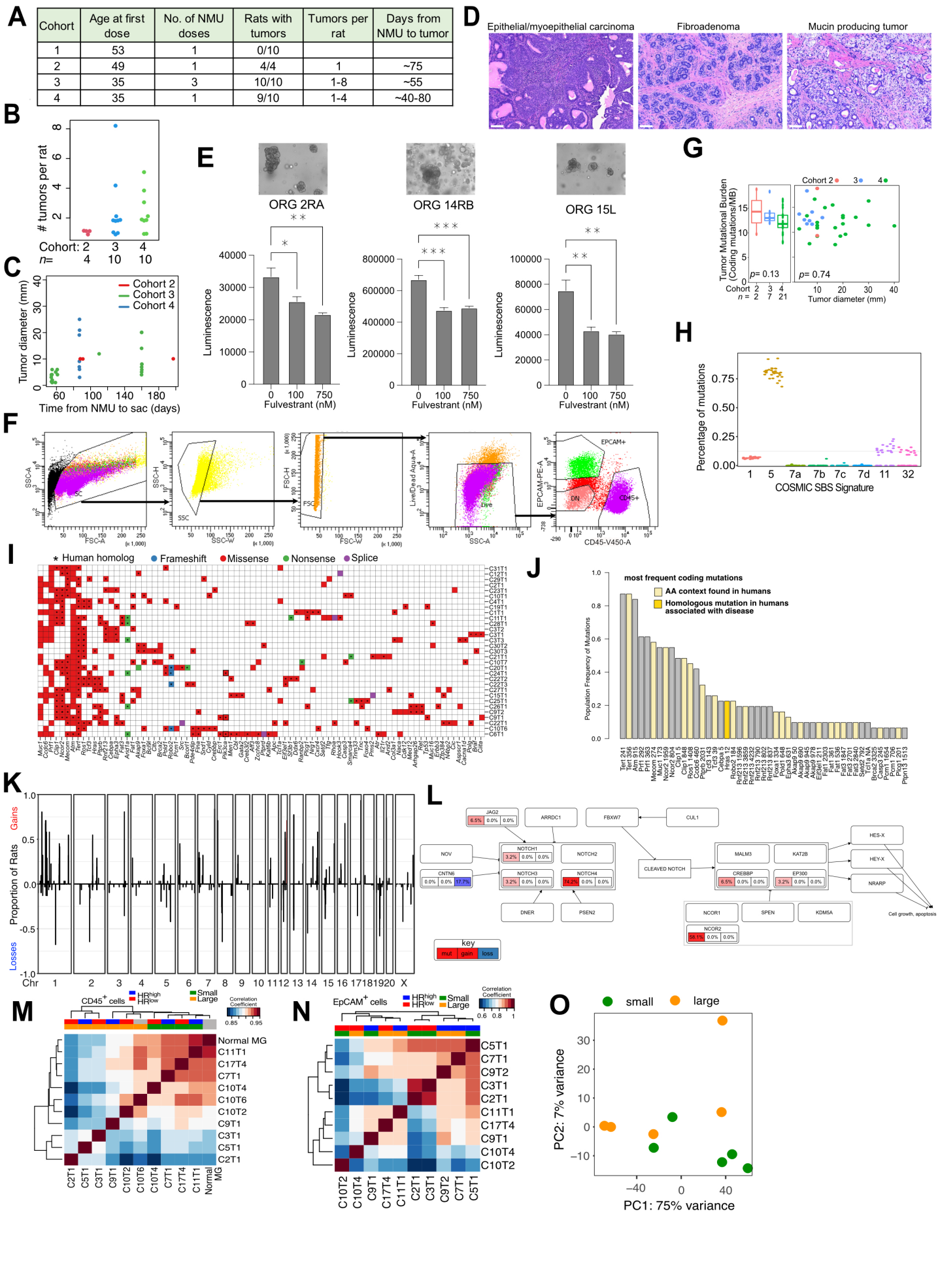

Supplementary Figure S1. Molecular characterization of NMU-induced mammary tumors. A, Summary of NMU treatment schedules, number of rats, and tumor latency and incidence. **B,** Number of tumors per rat. **C**, Variation in tumor diameter at time of collection after NMU-tumor induction. **D**, Hematoxylin-eosin staining of NMU-induced mammary tumors with different histology. **E** Representative images of organoid cultures (top) and graphs depicting luminescence signal of cultures treated with DMSO or fulvestrant. P-values were determined by One-way ANOVA with multiple comparisons tests. Representative results from n=2 experiments. **F**, Gating strategy used for FACS of $EpCAM^+$ tumor epithelial cells. SSC, side scatter, FSC, forward scatter. **G**, Total mutational burden association with cohort and size. Quartiles and range are shown. *p*-values calculated by Mann Whitney Wilcoxon test between cohort 3 and 4, and spearman correlation with size. **H**, Frequency of COSMIC SBS mutational signatures. **I,** Common mutations found in COSMIC genes. **J**, Most frequent coding mutations in the rat cohort. **K**, Genome-wide summary of the frequency of copy number variations in the rat characterization cohort. Gains and losses were defined as a log2(fold change) of ±0.3. **L**, Population frequency of genetic aberrations in NOTCH signaling pathway. **M-O**, Correlation between RNA-seq samples from $CD45^+$ (**M**) and $EpCAM^+$ (**N**) cell populations. Red and blue indicates HR^{low} and HR^{high} tumor, respectively. Green and orange marks small and large tumor, respectively. **O,** Principal component analysis of RNA-seq data of $EpCAM^+$ tumor cells from small and large tumors.

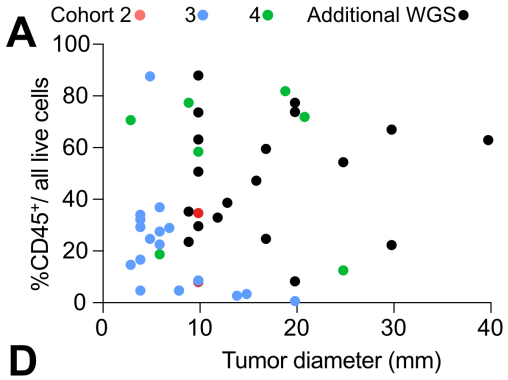
A
Cohort 2
3
4
Additional WGS
%CD45+/ all live cells
Tumor diameter (mm)

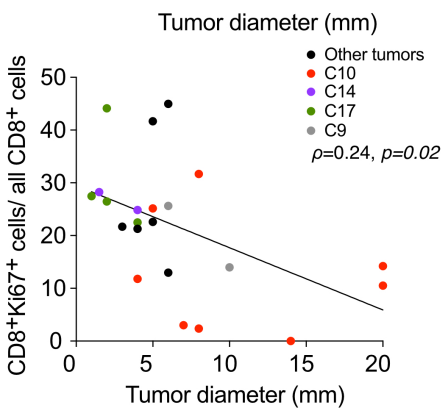
D
Other tumors
C10
C14
C17
C9
ρ=0.24, p=0.02
CD8+Ki67+ cells/ all CD8+ cells
Tumor diameter (mm)

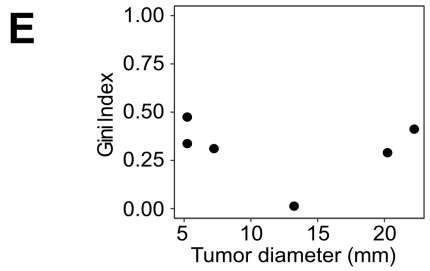
E
Gini Index
Tumor diameter (mm)

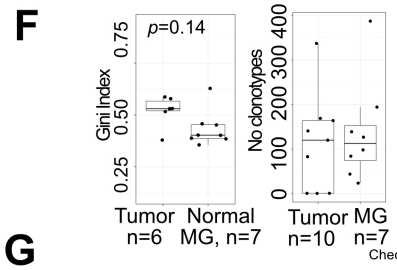
F
p=0.14
Gini Index
No clonotypes
Tumor n=6
Normal MG, n=7
Tumor n=10
MG n=7

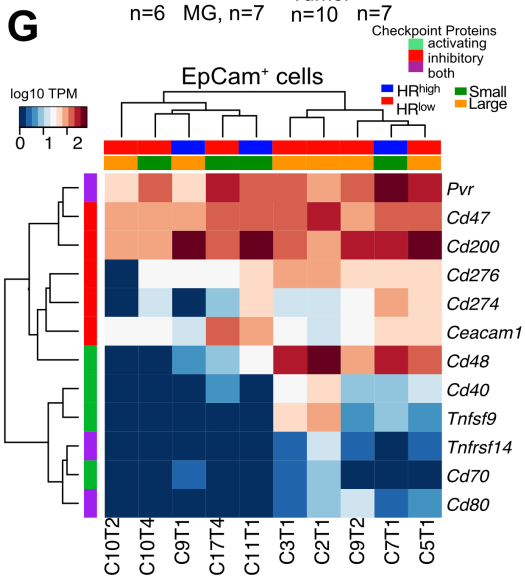
G
EpCam+ cells
log10 TPM
Checkpoint Proteins
activating
inhibitory
both
HRhigh
HRlow
Small
Large
Pvr
Cd47
Cd200
Cd276
Cd274
Ceacam1
Cd48
Cd40
Tnfsf9
Tnfrsf14
Cd70
Cd80
C10T2
C10T4
C9T1
C17T4
C11T1
C3T1
C2T1
C9T2
C7T1
C5T1

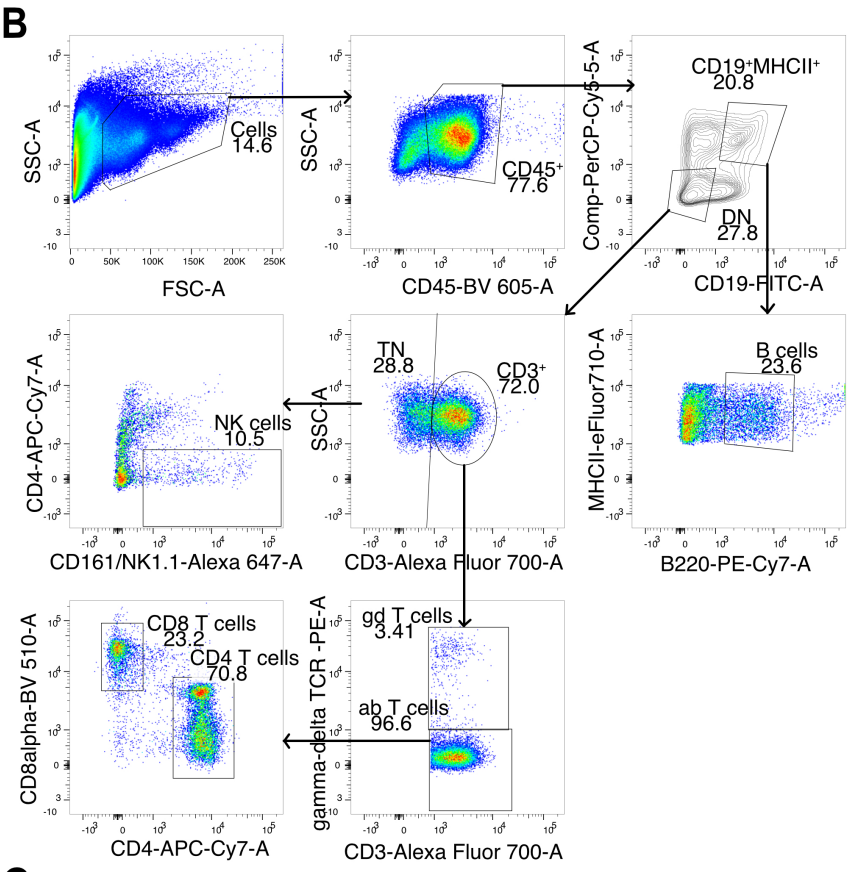
B
Cells 14.6
CD45+ 77.6
CD19+MHCII+ 20.8
DN 27.8
NK cells 10.5
TN 28.8
CD3+ 72.0
B cells 23.6
CD8 T cells 23.2
CD4 T cells 70.8
gd T cells 3.41
ab T cells 96.6
FSC-A
SSC-A
CD45-BV 605-A
CD19-FITC-A
CD161/NK1.1-Alexa 647-A
CD3-Alexa Fluor 700-A
B220-PE-Cy7-A
CD4-APC-Cy7-A

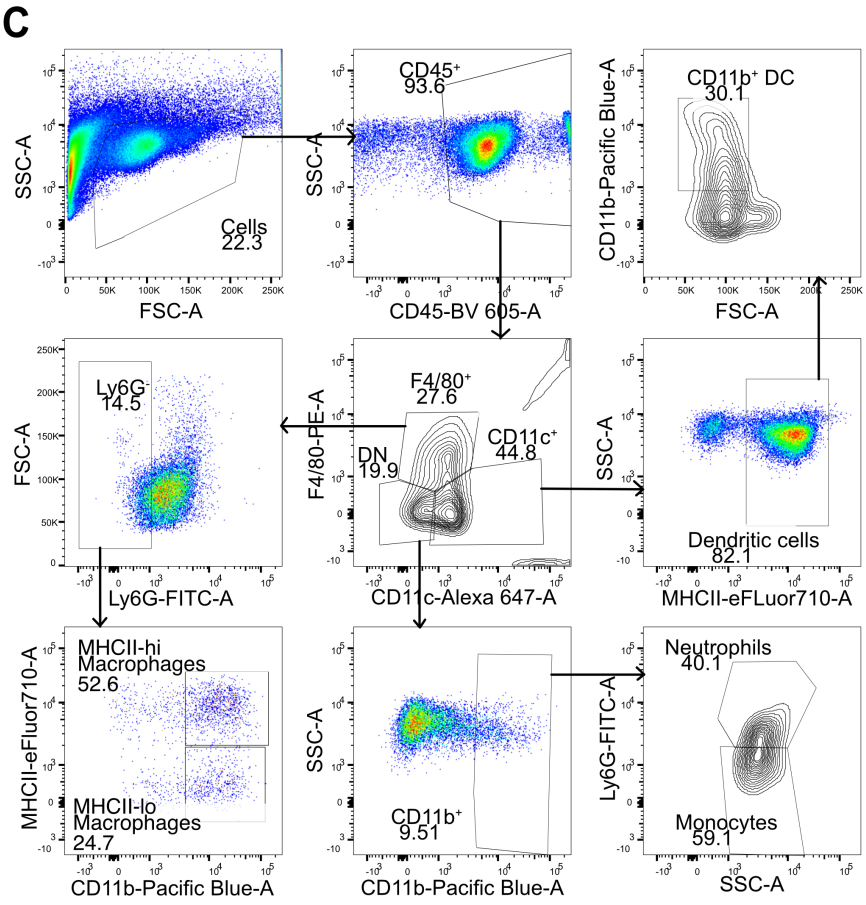
C
Cells 22.3
CD45+ 93.6
CD11b+ DC 30.1
Ly6G+ 14.5
F4/80+ 27.6
DN 19.9
CD11c+ 44.8
Dendritic cells 82.1
MHCII-hi Macrophages 52.6
MHCII-lo Macrophages 24.7
CD11b+ 9.51
Neutrophils 40.1
Monocytes 59.1
FSC-A
SSC-A
CD45-BV 605-A
CD11b-Pacific Blue-A
Ly6G-FITC-A
F4/80-PE-A
CD11c-Alexa 647-A
MHCII-eFLuor710-A

Supplementary Figure S2. The immune environment of NMU-induced mammary tumors. Red and blue indicates HR^{low} and HR^{high} tumor, respectively. Green and orange marks small and large tumors, respectively. **A,** Abundance of the $CD45^+$ cell population in tumors by FACS. **B-C,** Gating strategy used for polychromatic FACS to quantify the relative abundance of major cell types contributing to adaptive (**B**) and innate immunity (**C**). SSC, side scatter. FSC, forward scatter. DN, double negative. **D,** Correlation between the frequency of $Ki67^+CD8^+$ T cells determined by immunofluorescence and tumor diameter. For animals with multiple tumors, the tumors are shown in the same color. Animals that have just one tumor are shown in black. **E**, Correlation between BCR Gini index and tumor size. **F**, TCR Gini index and number of unique clonotypes in $CD45^+$ cells from tumors and mammary glands **G**, Heatmap of log_{10}TPM counts of immune checkpoint genes in $EpCAM^+$ tumor cells.

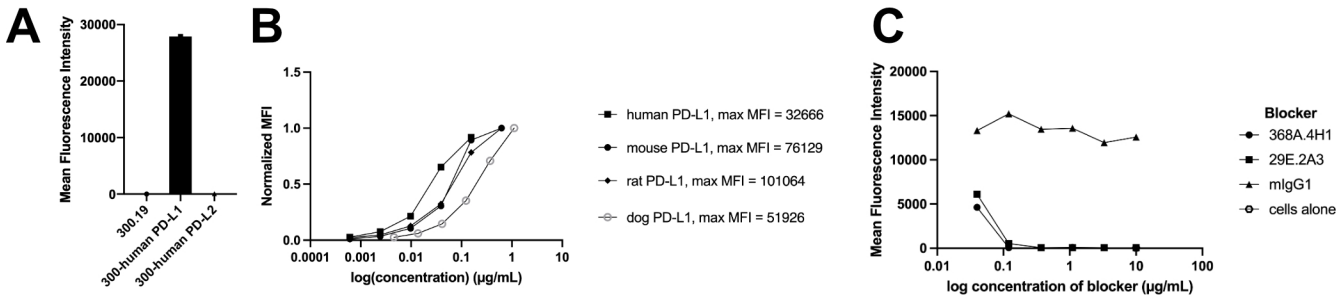

D

368A.4H1 VH

Protein

DVQLQESGPGLVKPSQSLSLTCTVTDYSITSDYAWTWIRQFPGNKLEWMGYITYRGTTRYNPSLTSRISFTRDTSKNQLFLQLNSVTTEDTGTYCCARSMITTGYYAMDYWG
QGTSVTVSS

DNA

GATGTGCAGCTTCAGGAGTCGGGACCTGGCCTGGTGAAACCTTCTCAGTCTCTGTCCCTCACCTGCACTGTCACTGACTACTCAATCACCAGTGATTATGCCTGGACCTGGA
TCCGGCCAGTTTCCGGGAAACAAACTGGAGTGGATGGGCTACATAACCTACAGAGGTACCACTCGCTACAACCCATCTCTCACAAGTCGAATCTCTTTCACTCGAGACACATC
CAAGAACCAGCTCTTCCTGCAGTTGAATTCTGTGACTACTGAGGACACAGGCACATATTGCTGTGCAAGATCTATGATTACGACGGGGTACTATGCTATGGACTACTGGGGT
CAAGGAACCTCAGTCACCGTCTCCTCA

368A.4H1 VK

Protein

DIVMTQSHKFMSTSVGDRVSISCKASQDVGISVAWYQQKPGQSPKLLIYWASTRHTGVPVRFTGSGSGTDFTLTISNVQSEDLADYFCQQYSSYPPTFGAGTKLELK

DNA

GACATTGTGATGACCCAGTCTCACAAATTCATGTCCACATCAGTAGGAGACAGGGTCAGCATCTCCTGCAAGGCCAGTCAGGATGTGGGTATTTCTGTAGCCTGGTATCAAC
AGAAACCAGGGCAATCTCCTAAACTACTGATTTACTGGGCATCCACCCGGCACACTGGAGTCCCTGTTCGCTTCACAGGCAGTGGATCTGGGACAGATTTCACTCTCACCAT
AAGCAATGTGCAGTCTGAAGACTTGGCAGATTATTTTTGTCAGCAGTATAGCAGTTATCCGCCCACGTTCGGTGCTGGGACCAAGCTGGAGCTGAAA

Supplementary Figure S3. Characterization of 368A.4H1 antibody. A, Reactivity of 368A.4H1 with human PD-L1 and PD-L2. 368A.4H1 mAb was incubated with untransfected 300.19 cells or 300.19 cells stably transfected with human PD-L1 or human PD-L2, washed, incubated with goat anti-mouse IgG-PE, washed, and analyzed by flow cytometry. **B,** Reactivity of 368A.4H1 with human, mouse, rat, and dog PD-L1. The indicated concentrations of 368A.4H1 mAb were incubated with 300.19 cells stably transfected with human, mouse, rat, or dog PD-L1, washed, incubated with goat anti-mouse IgG-PE, washed, and analyzed by flow cytometry. The mean fluorescence intensity was normalized to the maximal mean fluorescence intensity of that cell line = 1. From the EC50, the apparent affinity of 368A.4H1 for human, mouse, rat, or dog is 0.13, 0.27, 0.30, and 1.71 nM, respectively. **C,** Blockade of PD-1 binding to PD-L1 by 368A.4H1. Blockade of PD-1 binding to PD-L1 was assessed using a FACS-based assay. The indicated concentrations of 368A.4H1, 29E.2A3, or MOPC-31C mIgG1 isotype control were mixed with 300.19 cells expressing human PD-L1 and incubated at 4° C for 30 minutes. The cells were washed, then incubated for 30 minutes with human PD-1 ectodomain/human IgG1 fusion protein, washed, then incubated for 30 minutes with PE labeled goat-anti-human IgG antibody (multi-species absorbed), washed, and PD-1 binding was detected by flow cytometry. **D,** Sequence of 368A.4H1.

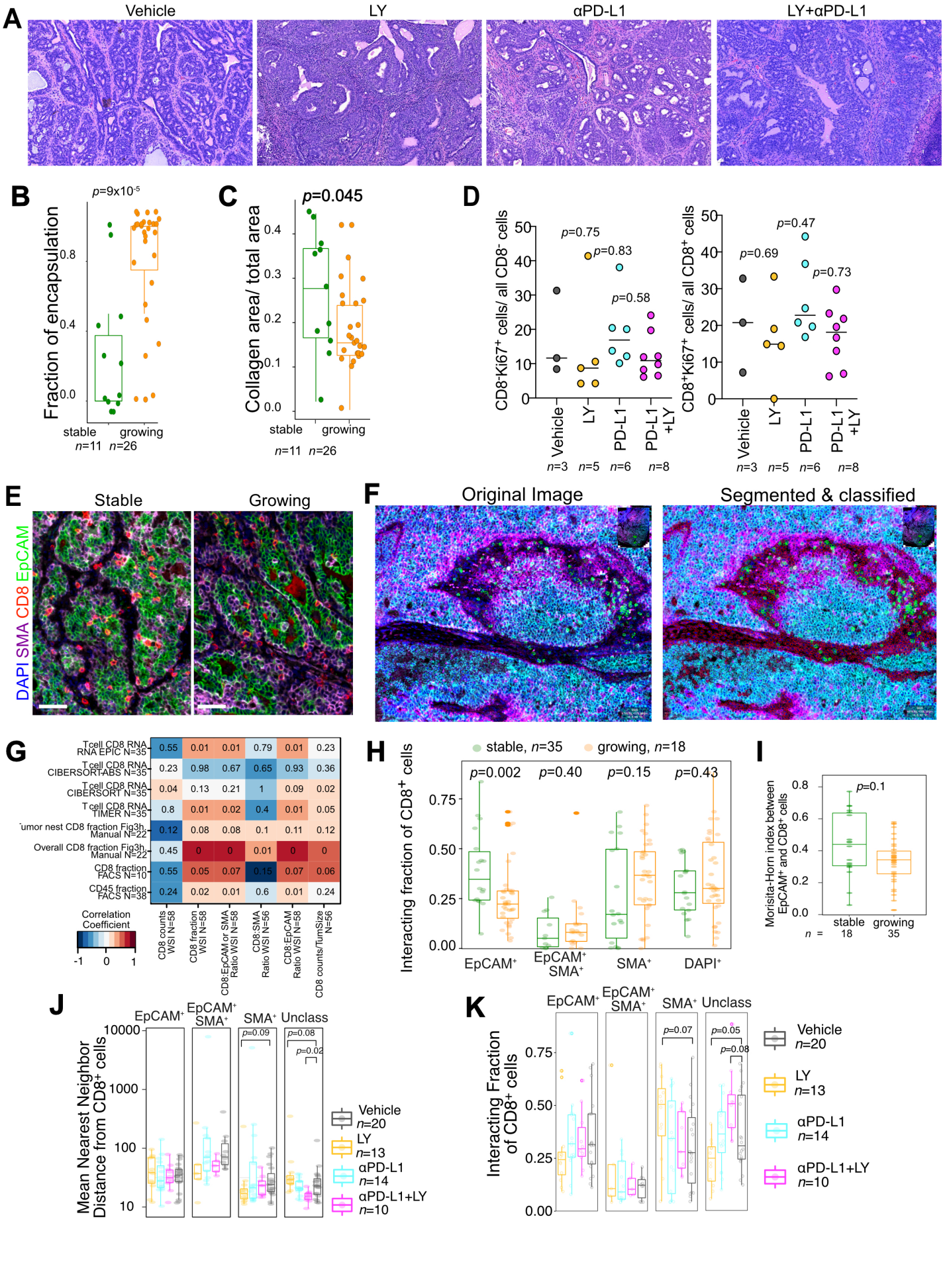
A
Vehicle
LY
αPD-L1
LY+αPD-L1
B
p=9x10-5
Fraction of encapsulation
stable
growing
n=11 n=26
C
p=0.045
Collagen area/ total area
stable
growing
n=11 n=26
D
CD8+Ki67+ cells/ all CD8- cells
p=0.75
p=0.83
p=0.58
Vehicle
LY
PD-L1
PD-L1 +LY
n=3 n=5 n=6 n=8
CD8+Ki67+ cells/ all CD8+ cells
p=0.69
p=0.47
p=0.73
Vehicle
LY
PD-L1
PD-L1 +LY
n=3 n=5 n=6 n=8
E
Stable
Growing
DAPI SMA CD8 EpCAM
F
Original Image
Segmented & classified
G
Tcell CD8 RNA RNA EPIC N=35
Tcell CD8 RNA CIBERSORT-ABS N=35
Tcell CD8 RNA CIBERSORT N=35
Tcell CD8 RNA TIMER N=35
Tumor nest CD8 fraction Fig3h Manual N=22
Overall CD8 fraction Fig3h Manual N=22
CD8 fraction FACS N=10
CD45 fraction FACS N=38
CD8 counts WSI N=58
CD8 fraction WSI N=58
CD8:EpCAM or SMA Ratio WSI N=58
CD8:SMA Ratio WSI N=56
CD8:EpCAM Ratio WSI N=58
CD8 counts/TumSize N=56
Correlation Coefficient
-1 0 1
H
stable, n=35
growing, n=18
Interacting fraction of CD8+ cells
p=0.002
p=0.40
p=0.15
p=0.43
EpCAM+
EpCAM+ SMA+
SMA+
DAPI+
I
Morisita-Horn index between EpCAM+ and CD8+ cells
p=0.1
stable
growing
n = 18 35
J
Mean Nearest Neighbor Distance from CD8+ cells
EpCAM+
EpCAM+ SMA+
SMA+
Unclass
p=0.09
p=0.08
p=0.02
Vehicle n=20
LY n=13
αPD-L1 n=14
αPD-L1+LY n=10
K
Interacting Fraction of CD8+ cells
EpCAM+
EpCAM+ SMA+
SMA+
Unclass
p=0.07
p=0.05
p=0.08
Vehicle n=20
LY n=13
αPD-L1 n=14
αPD-L1+LY n=10

Supplementary Figure S4. Microenvironmental analysis of NMU-induced tumors following immunotherapy. A, Representative pictures of H&E staining of tumors from different treatment groups. **B,** Fraction of encapsulation determined by manual semi-quantitative scoring of trichrome stained slides in growing and stable tumours. Shown are quartiles and range. *p*-values calculated using Mann Whitney Wilcoxon test. **C**, Quantification of collagen content in stable and growing tumors based on trichrome staining. Shown are quartiles and range. *p*-values calculated using Mann Whitney Wilcoxon test. **D**, Quantification of Ki67 in $CD8^-$ and $CD8^+$ cell populations based on immunofluorescence. Shown are quartiles and range. *p*-values calculated using Mann Whitney Wilcoxon test. **E,** Representative fields from whole slide scanning of immunofluorescence analysis of DAPI, SMA, CD8, and EpCAM in growing and stable tumors, scale bar, 100 μm. **F,** Example of automatic segmentation and classification of whole slide images (WSI) of immunofluorescence for SMA, CD8, and EpCAM. **G,** Correlation between WSI and other techniques including manual counting, FACS, and RNA-seq-based deconvolution. Color scale bar depicts Spearman correlation coefficient and numbers shown are corresponding p-values. **H,** Fraction of $CD8^+$ T cells within 15μm of indicated cell types stratified according to growth status. **I**, Morisita-Horn index between $CD8^+$ and $EpCAM^+$ cells in a 200 μm matrix. Quartiles and range are shown. *p*-values were calculated using the Mann Whitney Wilcoxon test. **J-K**, Spatial analysis between $CD8^+$ T cells and all other cell types stratified according to treatment. Quartiles and range are shown. *p*-values calculated by Wilcoxon-rank sum test. (**J),** Nearest neighbor distances. (**K),** Fraction of $CD8^+$ T cells within 15μm.

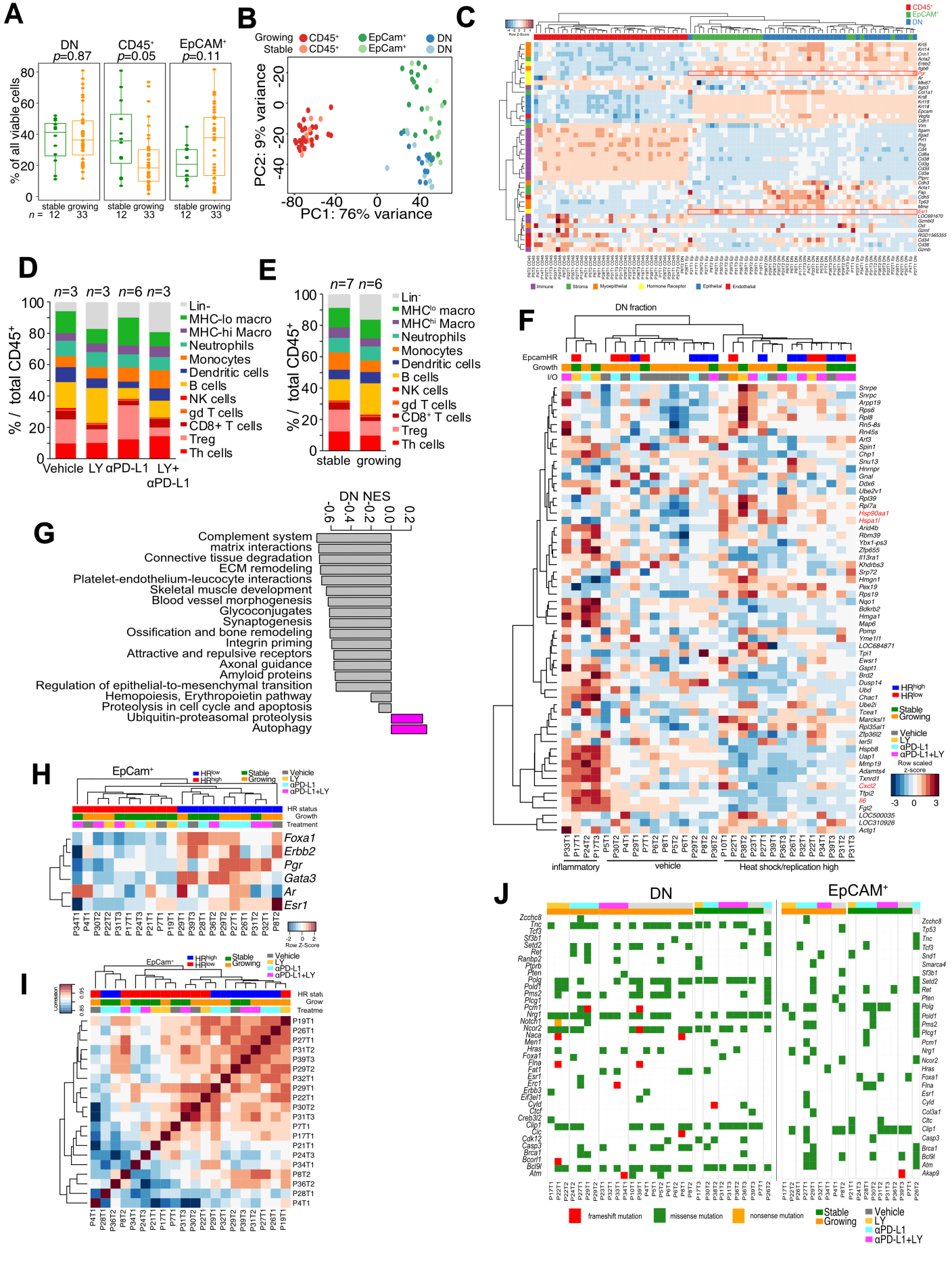
A
DN
p=0.87
CD45+
p=0.05
EpCAM+
p=0.11
% of all viable cells
stable growing
n = 12 33
B
Growing CD45+ EpCam+ DN
Stable CD45+ EpCam+ DN
PC2: 9% variance
PC1: 76% variance
C
CD45+
EpCAM+
DN
Immune
Stroma
Myoepithelial
Hormone Receptor
Epithelial
Endothelial
D
n=3 n=3 n=6 n=3
% / total CD45+
Lin-
MHC-lo macro
MHC-hi Macro
Neutrophils
Monocytes
Dendritic cells
B cells
NK cells
gd T cells
CD8+ T cells
Treg
Th cells
Vehicle
LY
αPD-L1
LY+ αPD-L1
E
n=7 n=6
% / total CD45+
Lin-
MHClo macro
MHChi Macro
Neutrophils
Monocytes
Dendritic cells
B cells
NK cells
gd T cells
CD8+ T cells
Treg
Th cells
stable
growing
F
DN fraction
EpcamHR
Growth
I/O
HRhigh
HRlow
Stable
Growing
Vehicle
LY
αPD-L1
αPD-L1+LY
Row scaled
Z-score
inflammatory
vehicle
Heat shock/replication high
G
DN NES
Complement system
matrix interactions
Connective tissue degradation
ECM remodeling
Platelet-endothelium-leucocyte interactions
Skeletal muscle development
Blood vessel morphogenesis
Glycoconjugates
Synaptogenesis
Ossification and bone remodeling
Integrin priming
Attractive and repulsive receptors
Axonal guidance
Amyloid proteins
Regulation of epithelial-to-mesenchymal transition
Hemopoiesis, Erythropoietin pathway
Proteolysis in cell cycle and apoptosis
Ubiquitin-proteasomal proteolysis
Autophagy
H
EpCam+
HR status
Growth
Treatment
Foxa1
Erbb2
Pgr
Gata3
Ar
Esr1
Row Z-Score
I
EpCam+
Correlation
J
DN
EpCAM+
frameshift mutation
missense mutation
nonsense mutation
Stable
Growing
Vehicle
LY
αPD-L1
αPD-L1+LY

Supplementary Figure S5. Molecular profiling of immunotherapy treated tumors. A, Frequencies of the indicated cell types determined by FACS in growing and stable tumors. Shown are quartiles and range. P-values calculated using Mann Whitney Wilcoxon test. **B**, Principal component analysis of $CD45^+$, $EpCAM^+$, and DN cell populations profiled by RNA-seq. **C**, Heatmap of row-normalized Z-scores of genes differentiating $CD45^+$, $EpCAM^+$, and DN cell populations. *Esr1* and *Pgr* is highlighted in red. **D-E**, Leukocyte composition of tumors by polychromatic flow cytometry classified by treatment (**D**) or by growth status (**E**). **F**, Heatmap of row-normalized Z-scores of differentially expressed genes between vehicle and all immunotherapy-treated tumors in the DN cell population. **G**, Normalized GSEA enrichment scores of significantly enriched pathways in vehicle vs. LY+PD-L1 treated DN cells. Gray and violet bars depict pathways enriched in vehicle and LY+PD-L1 tumors, respectively. **H**, Row-normalized Heatmap of HR-related genes including luminal transcription factors. **I**, Spearman correlations between $EpCAM^+$ RNA-seq samples. **J**, Common cancer mutations in RNA-seq from in $EpCAM^+$ and DN cells. Red and blue color indicates HR^{low} and HR^{high} tumors, respectively. Green and orange color marks stable and growing tumors, respectively.

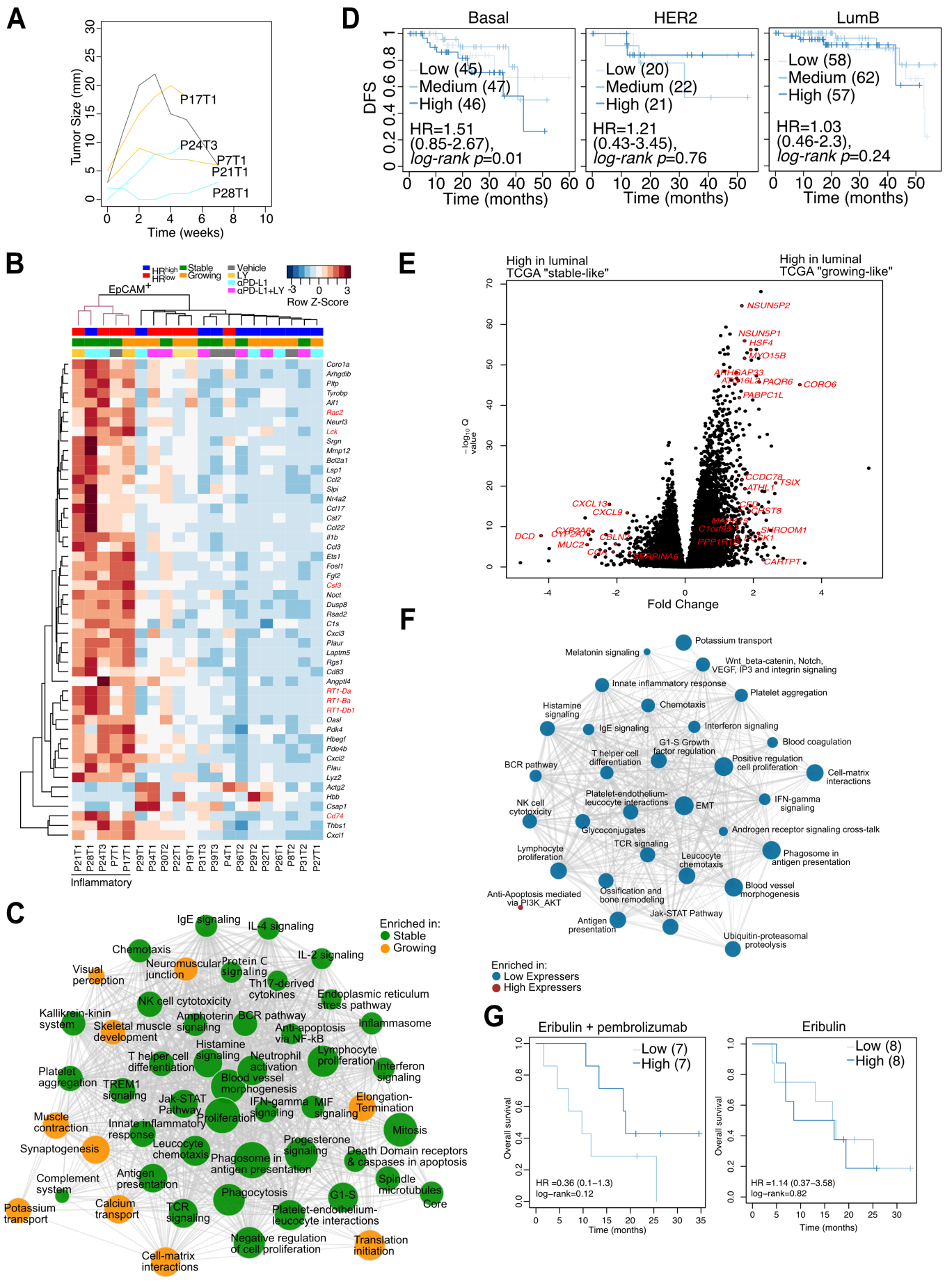
A
Tumor Size (mm)
Time (weeks)
P17T1
P24T3
P7T1
P21T1
P28T1
D
Basal
HER2
LumB
DFS
Low (45)
Medium (47)
High (46)
HR=1.51
(0.85-2.67),
log-rank p=0.01
Low (20)
Medium (22)
High (21)
HR=1.21
(0.43-3.45),
log-rank p=0.76
Low (58)
Medium (62)
High (57)
HR=1.03
(0.46-2.3),
log-rank p=0.24
Time (months)
B
HRhigh
HRlow
Stable
Growing
Vehicle
LY
aPD-L1
aPD-L1+LY
Row Z-Score
EpCAM+
Inflammatory
E
High in luminal
TCGA "stable-like"
High in luminal
TCGA "growing-like"
Fold Change
F
Potassium transport
Melatonin signaling
Wnt_beta-catenin, Notch,
VEGF, IP3 and integrin signaling
Innate inflammatory response
Platelet aggregation
Chemotaxis
Histamine signaling
IgE signaling
Interferon signaling
Blood coagulation
G1-S Growth factor regulation
T helper cell differentiation
BCR pathway
Positive regulation cell proliferation
Cell-matrix interactions
Platelet-endothelium-leucocyte interactions
EMT
IFN-gamma signaling
NK cell cytotoxicity
Glycoconjugates
Androgen receptor signaling cross-talk
TCR signaling
Lymphocyte proliferation
Leucocyte chemotaxis
Phagosome in antigen presentation
Anti-Apoptosis mediated via PI3K_AKT
Ossification and bone remodeling
Blood vessel morphogenesis
Antigen presentation
Jak-STAT Pathway
Ubiquitin-proteasomal proteolysis
Enriched in:
Low Expressers
High Expressers
C
IgE signaling
IL-4 signaling
Chemotaxis
Neuromuscular junction
Protein C signaling
IL-2 signaling
Visual perception
Th17-derived cytokines
Endoplasmic reticulum stress pathway
NK cell cytotoxicity
Kallikrein-kinin system
Amphoterin signaling
BCR pathway
Inflammasome
Skeletal muscle development
Anti-apoptosis via NF-kB
Histamine signaling
Lymphocyte proliferation
T helper cell differentiation
Neutrophil activation
Platelet aggregation
Blood vessel morphogenesis
Interferon signaling
TREM1 signaling
Jak-STAT Pathway
IFN-gamma signaling
MIF signaling
Elongation-Termination
Proliferation
Muscle contraction
Innate inflammatory response
Mitosis
Progesterone signaling
Leucocyte chemotaxis
Synaptogenesis
Phagosome in antigen presentation
Death Domain receptors & caspases in apoptosis
Antigen presentation
Spindle microtubules
Complement system
Phagocytosis
G1-S
Core
Potassium transport
Calcium transport
TCR signaling
Platelet-endothelium-leucocyte interactions
Negative regulation of cell proliferation
Translation initiation
Cell-matrix interactions
Enriched in:
Stable
Growing
G
Eribulin + pembrolizumab
Low (7)
High (7)
HR =0.36 (0.1–1.3)
log–rank=0.12
Eribulin
Low (8)
High (8)
HR =1.14 (0.37–3.58)
log–rank=0.82
Overall survival
Time (months)

Supplementary Figure S6. Characterization of EpCAM$^+$ specific differences between stable and growing tumors. Red and blue designation represents HR^{low} and HR^{high} tumors, respectively. Green and orange color marks stable and growing tumors, respectively. **A**, Growth curves of inflammatory tumors. **B**, Row-normalized heatmap of inflammation-related genes in the EpCAM$^+$ cell population. **C**, Enriched pathways in HR^{high} growing vs. stable tumors. Node size indicates the number of genes within the pathway, line width reflects the number of shared genes between two gene sets. **D,** Disease-free survival plots of TCGA basal, HER2, and LumB breast cancer patients segregated by the "Luminal growing" gene signature. Dark, medium, and light curves represent terciles with high, medium, and low expression of the signature, respectively. Hazard Ratio and 95% confidence interval were computed by modeling the signature score as a continuous variable in a cox model accounting for stage. *P*-values were calculated using log-rank test. **E**, Volcano plot of genes differentially expressed in the TCGA Luminal A tumors with high or low expression the "Luminal-growing" rat tumor gene signature. Selected immune-related genes in red have a [Log2 fold change]>1.5 and adjusted p-value<0.05. **F,** Pathways enriched in TCGA LumA with high and low expression of the "Luminal-growing" signature. Node size indicates the number of genes within the pathway, line width reflects the number of shared genes between two gene sets. **G,** Kaplan Meier plots of overall survival segregated by high and low "Luminal-growing" signature in an ER$^+$ metastatic breast cancer cohort treated with eribulin+pembrolizumab or eribulin alone. Low and high arms dichotomized using the median value and used in a univariate cox model to report Hazards ratio with 95% confidence intervals. P-values calculated using log-rank test.

SUPPLEMENTARYTABLES

Supplementary Table S1. Description of antibodies used.

Supplementary Table S2. Description of animals used for characterisation and immunotherapy cohorts.

Supplementary Table S3. Coding mutations in NMU cohort as profiled by whole genome sequencing.

Supplementary Table S4. List of differentially expressed genes across different comparisons. Gene Set Enrichment Analysis of DGE results. Gene signature associated with tumor growth or progression in HR^{high} tumors.